**Annals of Pharmacy Practice and Pharmacotherapy**
**ISSN: 3062-4436**
2021, Volume 1, Page No: 171-181

Available online at: www.galaxypub.co/page/journals

Galaxy Publication

Galaxy Publication

# Development of a Customizable, Near Real-Time TEER System for Dynamic Barrier Function Analysis

**Ahmed A. Al-Harbi[1], Khalid S. Alotaibi[1], Mohammed N. Alzahrani[1]***

[1]Department of Clinical Pharmacy, College of Pharmacy, King Saud University, Riyadh, Saudi Arabia.

***E-mail** ✉ m.alzahrani.pharm@gmail.com

**Received:** 16 May 2021; **Revised:** 04 August 2021; **Accepted:** 09 August 2021

## ABSTRACT

Barrier tissues, particularly the endothelium, play a central role in controlling substance exchange across the body. Trans-endothelial/epithelial electrical resistance (TEER) serves as a key bioelectrical indicator of barrier function. While commercial TEER systems exist, they are typically costly, large, and difficult to adapt to specialized experimental configurations such as microfluidic platforms. Building on our previous Arduino-based TEER sensor, this work introduces a significantly improved generation featuring: 1) a wide measurement range of 242–11, 880 Ω·cm² with excellent accuracy (>95%), suitable for most TEER applications, 2) integration with a 3D-printed microfluidic platform that enables modular cell seeding and flow-based experiments, 3) programmable on-off measurement cycles to minimize electrical stress on cells, 4) fully automated long-term recordings with adjustable time intervals. Using this system, we examined the impact of doxorubicin on endothelial barrier function at 1-minute intervals over 24 hours. Endothelial toxicity represents an emerging and poorly understood aspect of cardiotoxicity. At a clinically relevant concentration, barrier integrity remained largely stable until ~16 hours, after which TEER values began to decline (indicating increased permeability), followed by partial recovery. At a higher concentration (2.5 μM), TEER decreased markedly after 5 hours and showed no recovery, suggesting significant endothelial damage. In summary, we introduce a versatile, low-cost TEER platform capable of continuous monitoring of drug effects on barrier tissues. Its adaptable design makes it suitable for diverse applications, including personalized drug dosing on stem-cell-derived barriers and studies of transient permeability changes in disease models.

**Keywords:** Sensor, TEER, Barrier tissues, Endothelium, Doxorubicin, Cardiotoxicity

**How to Cite This Article:** Al-Harbi AA, Alotaibi KS, Alzahrani MN. Development of a Customizable, Near Real-Time TEER System for Dynamic Barrier Function Analysis. Ann Pharm Pract Pharmacother. 2021;1:171-81. https://doi.org/10.51847/CduUYhr62z

## Introduction

Endothelial and epithelial layers create essential biological barriers throughout the organism. Endothelial cells form the inner lining of blood vessels (endothelium), while epithelial cells provide protective coverings on the external surfaces of many organs (epithelium) [1-3]. The tight junctions between these cells tightly regulate the passage of substances between the luminal and abluminal compartments, thereby maintaining whole-body homeostasis [4, 5]. Disruption of barrier function is associated with numerous pathological conditions, including Alzheimer's and Parkinson's diseases [6, 7].

In recent years, drug-induced endothelial damage has gained attention as an important but understudied dimension of cardiotoxicity [8]. However, there is currently no system capable of near real-time tracking of barrier integrity changes, and the time-dependent effects of many common drugs on these tissues remain poorly characterized. Such kinetic information is vital for optimizing drug efficacy, determining appropriate doses, and establishing optimal dosing schedules [9].

Trans-endothelial/epithelial electrical resistance (TEER) is a widely accepted method for assessing barrier tightness. TEER reflects the electrical resistance across a cell monolayer: a well-formed, tightly packed layer

restricts ion movement and yields high TEER values, whereas a compromised layer allows greater ion flow and produces lower readings [10].

Commercial TEER instruments, while available, are generally expensive, cumbersome, and offer limited adaptability to custom experimental setups [11, 12]. This often forces researchers to adapt their protocols to the equipment rather than the other way around. Several research groups have therefore developed affordable, customizable TEER devices tailored to specific needs [13].

In this work, we describe an enhanced TEER sensor prototype that can be easily constructed using Arduino, allows flexible electrode configurations, supports flow and shear stress studies through a coupled modular microfluidic system, incorporates programmable current on-off cycles to protect cells, and enables automated long-term monitoring with user-defined measurement intervals.

To illustrate its capabilities, we thoroughly characterized the device and then applied it to study the dynamic effects of the widely used anticancer drug doxorubicin on endothelial barrier function at 1-minute resolution. We observed that a clinically relevant concentration (0.5 μM) [14] caused only minor TEER reduction after 16 hours, followed by partial recovery of barrier integrity. In contrast, a higher concentration (2.5 μM) triggered a substantial TEER decline after 5 hours that persisted without recovery over 24 hours. To our knowledge, this represents the first near real-time demonstration of doxorubicin's dynamic impact on endothelial permeability.

The presented TEER platform holds strong potential for broader drug toxicity screening.

## Materials and Methods

*Assembly of the TEER circuitry*

Three independent TEER circuits (each with a dedicated sensor) were built on breadboards. Power was supplied by a 5 V AC wall adapter (Model 2230651, Jameco Electronics, Belmont, CA, USA) delivering 60 Hz alternating current. The positive terminal of the AC source was connected to pin 6 of a solid-state relay (SSR) (PVT212PBF, Digikey, Bloomington, MN, USA). Pin 4 of the SSR was wired in series to two precision resistors (measured at 33, 100 Ω and 15, 000 Ω using a calibrated multimeter) and then to two jumper leads that served as connections to the TEER electrodes. This arrangement formed a voltage divider, allowing calculation of the resistance between the electrodes via Ohm's law [15]. The second electrode lead was directly linked to the negative terminal of the AC supply. A 1 kΩ resistor connected pin 1 of the SSR to a digital output pin on an Arduino Due microcontroller (Arduino, Somerville, MA, USA), while pin 2 was grounded. Two additional jumper wires—one taken before the first electrode lead and one from the AC negative terminal—were routed to a full-wave bridge rectifier built from four Schottky diodes (112-SB110-E3/54CT-ND, Digikey, Bloomington, MN, USA) to convert the AC signal to DC [16]. The rectified output was grounded and fed into an analog input of the Arduino for voltage monitoring and data logging. To reduce signal noise, a smoothing capacitor was incorporated, with different capacitance values evaluated for optimal performance.

*Preparation of electrodes*

Pairs of platinum electrodes were produced within custom 3D-printed holders for seamless incorporation into the microfluidic system. The holder designs were created in Autodesk Inventor and fabricated using a Formlabs Form 3B printer (Formlabs, Somerville, MA, USA). Each holder featured a central 1 mm diameter channel to accommodate the electrode wire. A 3 cm length of 0.25 mm diameter platinum wire (Product No.: 010288-CC, Thermo Fisher Scientific, Rockville, MD, USA) was inserted into the channel, fixed with transparent epoxy, and cured overnight. The exposed tip of each electrode assembly was then smoothed using a belt sander equipped with 600-grit silicon carbide paper.

*Arduino software development*

Measurement acquisition and storage were implemented using the open-source Arduino IDE. The guide covers customization of key parameters such as channel count, measurement frequency, and experiment duration.

*Performance validation of the TEER system*

A calibration curve was generated by recording output voltage across a series of known resistors placed in the R3 position. Data from the three parallel sensors were averaged to produce the final calibration profile. Accuracy was assessed by testing resistors spanning the calibrated range and computing recovery as (measured resistance ÷ known resistance) × 100%. Dynamic response was evaluated by sequentially adding NaCl solutions (0.01 M to

0.5 M) to a reservoir containing the electrodes and immediately recording resistance changes under automated control.

*Design and assembly of the modular microfluidic platform*

Microfluidic components were modeled in Autodesk Inventor. The complete device adopted a cylindrical form (dimensions approximately 46 mm × 13 mm × 21.7 mm). In cross-section, it contained intersecting channels forming a cross pattern. The central segment consisted of a 450 μm × 5.5 mm slot designed to accommodate an endothelial-cell-seeded insert (described below). Flanking side channels measured 300 μm × 4.7 mm each, permitting fluid flow on both faces of the insert. Along the device axis, two ports were included to securely position the electrode holders, ensuring electrode contact with fluid in the side channels during TEER readings. The cylinder ends featured threaded connectors (0.75 mm diameter internal coil, 2 mm pitch, 10 mm depth) compatible with 3D-printed fingertight fittings for tubing attachment and perfusion. Fluid circulation was achieved using Tygon tubing (inner diameter 0.020", outer diameter 0.060"; Cole-Parmer, Vernon Hills, IL, USA) and peristaltic pump tubing with dual stoppers (inner diameter 0.64 mm; Cole-Parmer, Vernon Hills, IL, USA).

*Fabrication of cell culture inserts*

A laser cutter (Full Spectrum Laser, Las Vegas, NV, USA) operating in vector mode (17.1% vector current, 1.1% raster power, 1.1% raster speed) was used to excise 20 mm × 2.2 mm rectangular windows from 450 μm thick polystyrene sheets. Separately, a custom electrospinning setup [13] was employed to produce microfiber scaffolds from 15% (m/v) polycaprolactone dissolved in trifluoroethanol, collected on a mandrel rotating at ~4, 500 rpm. The resulting fibrous mats were aligned over the polystyrene windows. The assembly was returned to the laser cutter, where 30 mm × 5.1 mm rectangles were cut around each window, simultaneously heat-fusing the fibers to the polystyrene frame at the edges. Final insert width was intentionally undersized relative to the microfluidic slot to account for thermal distortion of polystyrene during laser processing.

*Cell culture procedures*

Inserts were sterilized by thorough 70% ethanol spraying followed by UV-assisted air drying. Eight inserts were arranged fiber-side up in a 60 mm Petri dish. Each was coated by applying 250 μL of 0.3 mg/mL sterile collagen solution (Millipore-Sigma, St. Louis, MO, USA) for 20 min at 4 °C, after which excess was removed and surfaces rinsed sequentially with PBS and 70% ethanol. Coated inserts were dried under UV illumination (385 nm, 100 mW) in a biosafety cabinet for 1 min. Passage 5 bovine pulmonary artery endothelial cells (BPAECs, ATCC, Manassas, VA, USA) were resuspended at ~750, 000 cells/mL (confirmed by hemocytometer) in DMEM, and 2 mL of suspension was dispensed across the inserts. After 30 min incubation for initial attachment, 6.5 mL additional DMEM was added to submerge the inserts. Medium was refreshed daily until confluent monolayers formed (~4 days).

*Assessment of doxorubicin's impact on endothelial barrier function*

The microfluidic platforms integrated with TEER sensors were placed inside a cell culture incubator (VWR, Suwanee, GA, USA), with continuous perfusion maintained by a peristaltic pump. Baseline TEER values were first established by circulating DMEM supplemented with 10% fetal bovine serum (FBS) and 1% penicillin-streptomycin through the channels at 800 μL/min for 2 h, in the absence of cell inserts. Perfusion was then stopped, and an endothelial-seeded insert was loaded into the central slot of the device. The Arduino was programmed to acquire data every minute throughout a 24-h experiment. For each acquisition cycle, power was applied to the circuit for 600 ms—including an initial 100 ms stabilization phase followed by 100 rapid samples taken at 5 ms intervals—while remaining off for the rest of the 59, 400 ms. The 100 samples were averaged to produce one voltage value per minute. At the 5-h mark, doxorubicin was added directly into the circulating medium via a calibrated micropipette to reach final concentrations of either 0.5 μM or 2.5 μM. Three independent setups were run simultaneously, corresponding to control, 0.5 μM, and 2.5 μM conditions. To verify that doxorubicin altered barrier integrity, inserts were carefully removed with tweezers at the end of the TEER recording period, fixed in 4% paraformaldehyde for 30 min, and then stained for 10 min with 0.5% (m/v) crystal violet in 25% methanol. Bright-field images were captured using a light microscope (Zeiss, Dublin, CA, USA), and intercellular gaps were quantified in ImageJ.

*Data processing and statistical evaluation*

Raw data were exported from the Arduino IDE serial monitor, which logged four columns: measurement time (in minutes) and voltage signals from each of the three parallel microfluidic devices. Data were imported into Microsoft Excel, where voltages were first converted to resistance using the individual calibration curve for each device, then multiplied by the effective endothelial area (0.44 cm², corresponding to the open window of the insert) to yield TEER in Ω·cm². The mean TEER obtained from initial blank runs (without cells) was subtracted to isolate the contribution from the cell monolayer. Results from four biological replicates were averaged, with standard deviations displayed as error bars. Statistical significance was assessed using t-tests, with differences considered significant at $P < 0.05$.

**Results and Discussion**

The developed platform combined an advanced TEER measurement system with a 3D-printed modular microfluidic setup, enabling near real-time monitoring of drug-induced changes in endothelial permeability.

*Hardware components of the TEER sensor*

*Circuit design*

As shown in **Figure 1a**, the setup comprised a primary measurement circuit and a rectification stage. The measurement segment consisted of three resistors in series: two fixed resistors (R1 = 33, 100 Ω; R2 = 15, 000 Ω) followed by the variable resistance of the cell monolayer (R3). This configuration operated as a voltage divider, permitting calculation of the monolayer resistance via Ohm's Law. Alternating current (AC) was chosen because it minimizes cell damage relative to direct current (DC) by reducing charging effects [17, 18]. Previous studies using both commercial and homemade systems have reported safe TEER measurements with currents ranging from 5 µA to 313 µA without harming monolayers [19-21]. To further ensure safety, our system activated the circuit for only 600 ms per minute, delivering currents of approximately 83–99 µA (verified with a calibrated multimeter), well below reported thresholds.

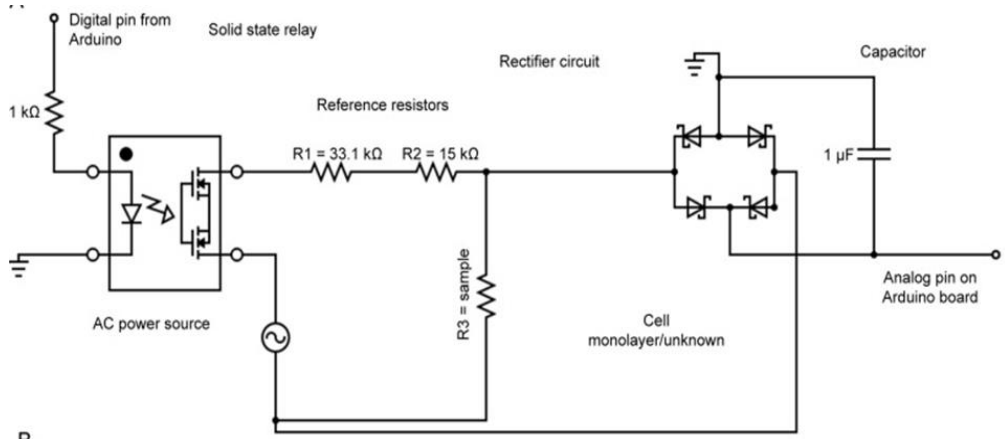


a)

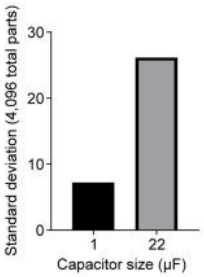


b)

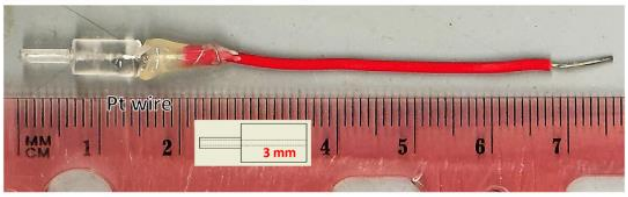


c)

**Figure 1.** Design of the trans-endothelial/epithelial electrical resistance (TEER) sensor. (a) Circuit schematic for one TEER channel, illustrating AC flow through fixed resistors (R1, R2) and the cell monolayer (R3). The voltage across R3 is captured, rectified to DC via a full-bridge circuit, and read by the Arduino. (b)

Comparison of signal stability (standard deviation) when using either a 1 μF or 22 μF capacitor in parallel with the rectifier. (c) Platinum wire embedded in a 3D-printed holder. Pairs of these electrodes spanned R3 (either standard resistors during validation or cell monolayers in doxorubicin experiments). Inset shows detailed positioning of the Pt wire inside the holder.

Furthermore, alternating current (AC) was utilized in the sensor design to mitigate the influence of electrical double layers at the electrode surface [22], which can introduce variability in resistance readings, particularly during prolonged monitoring. Direct current (DC) applied across electrodes in an aqueous environment progressively increases charge accumulation at the electrode-electrolyte boundary. Over time, this leads to charge buildup on both anode and cathode, as DC cannot periodically dissipate these charges [22-24]. This phenomenon effectively creates capacitive behavior at each interface, generating high impedance that interferes with accurate TEER assessment. In contrast, AC periodically reverses polarity, preventing significant double-layer formation and largely eliminating this artifact. A comparative test using DC in phosphate-buffered saline (PBS) revealed substantial signal drift over 30 h, whereas AC maintained a stable, flat response throughout the same period.
The rectifier stage transforms the AC output from the sensing circuit into DC, since the Arduino microcontroller cannot reliably process or interpret AC waveforms. Moreover, as the Arduino is unable to register negative voltages, the full-bridge rectifier—built from four diodes—routes current through alternate pathways for each half-cycle, folding both directions into positive polarity to yield usable DC. Nevertheless, this rectification produces residual ripple from the superimposed half-sine waves. To counteract this, a smoothing capacitor was connected across the rectifier output, releasing stored charge during low points to sustain steadier voltage [25]. Various capacitor values were evaluated by recording signals every second over 180 s, then computing the mean and standard deviation to identify the option yielding minimal variability. A 1 μF capacitor provided the greatest stability, with a standard deviation of 7.06 units (out of 4, 096), while a 22 μF capacitor produced greater variability at 25.93 units (out of 4, 096), as presented in **Figure 1b**. Residual minor fluctuations persisted even with capacitance smoothing, so the software was configured to acquire 100 rapid samples every 5 ms and compute their average for each final TEER value.

*Electrode design*

Conventional TEER setups typically employ paired electrodes, often Ag combined with Ag/AgCl types, placed on opposing sides of the cell monolayer to probe its resistance [10]. These are frequently configured as rigid chopstick-like probes with limited adaptability. Furthermore, prolonged experiments risk cytotoxicity from gradual release of $Ag^+$ ions from silver-based electrodes. To circumvent this issue, platinum wire was chosen for the present system. Platinum exhibits superior chemical inertness and a higher standard reduction potential of approximately 1.2 V versus the standard hydrogen electrode, compared to 0.79 V for silver [26, 27]. The slender platinum wires enable extensive customization, such as shaping, positioning, and securing via fingertight connectors, facilitating integration into diverse experimental configurations. As depicted in **Figure 1c**, the electrodes were housed in 3D-printed cylindrical holders that allowed simple, plug-and-play insertion into the microfluidic platform, with additional details provided later.

*Software implementation for the TEER sensor*

*Overall program structure*

The codebase is organized into three main sections: declaration of variables, initialization of the microcontroller, and the core acquisition routine. Floating-point variables were defined to handle non-integer values accurately.

*Microcontroller initialization*

The serial.begin() function established communication with the serial monitor at 9, 600 baud, a common default rate for Arduino boards. The pinMode() command designated specific digital pins as outputs to drive the solid-state relays (SSRs), enabling precise on/off control of current to the electrodes. Additionally, serial.println() statements were set up to label columns for time stamps and voltage readings in the output data.

*Data acquisition process*

At the start of each cycle, storage variables were reset to zero, and analogReadResolution() was configured for 12-bit precision to improve sensitivity over the default 10-bit mode. The Arduino quantizes voltage into discrete levels (parts). For the Arduino Due operating at 3.3 V reference, 12-bit resolution divides the range into 4, 096 parts, yielding a theoretical resolution of approximately 0.8 mV per step—four times finer than the 3.2 mV step in 10-bit mode (1, 024 parts). The digitalWrite() command then energized all three SSR channels simultaneously, followed by a 100 ms delay() pause to ensure circuit stabilization. A for loop subsequently captured 100 samples at 5 ms intervals over 500 ms, converting each raw reading to volts and storing it in an array. The array values were averaged to generate one consolidated voltage per time point. This multi-sample averaging further suppressed residual noise from the rectifier. After acquisition, the SSRs were deactivated to interrupt current flow, and the averaged voltages for each channel were transmitted to the serial monitor via serial.print(). The program then paused for 59, 400 ms before initiating the next cycle.

Overall, data points were collected at 1-minute intervals, with the circuit energized solely for the first 600 ms of each minute—comprising 100 ms for stabilization and 500 ms for the 100-sample burst. This duty cycle substantially limited electrical exposure to the cells while providing robust readings. The averaged value from each burst served as the recorded data point for that minute.

*Analytical validation of the TEER sensor*

*System calibration*

A calibration plot was first generated by recording voltage drops across the R3 position for a series of known resistors. As presented in **Figure 2a**, the mean curve obtained from three concurrent systems demonstrated excellent reproducibility and fitted a strong quadratic model. The lower limit of detection was set at 550 Ω, below which variability exceeded 10%. The upper quantitative limit was established at 27, 000 Ω; testing a 33, 000 Ω resistor produced a voltage near the Arduino's maximum of 3.3 V, risking signal saturation. Accounting for the effective cell area of the inserts, this resistance range translated to a TEER span of 242–11, 880 Ω·cm², encompassing the majority of values reported in typical endothelial/epithelial studies [17, 28, 29].

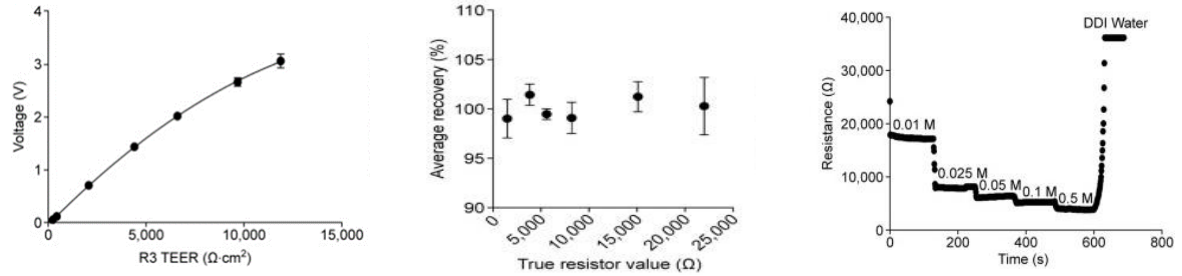


a) b) c)

**Figure 2.** Performance characterization of the sensor for precise resistance detection. (a) Calibration curve of the TEER system, showing measured voltage across R3 versus known resistance. The averaged data (n=3 parallel sensors) fitted the equation $y = –9.771 \times 10^{–9}x^2 + 0.0003751x – 0.04188$ with $R^2 = 0.9975$ (error bars = standard deviation). (b) Accuracy assessment via percent recovery across a range of resistors (1, 506; 3, 870; 5, 610; 8, 220; 15, 110; and 22, 000 Ω; averaged from three parallel sensors, error bars = standard deviation). (c) Dynamic response of the sensor to stepwise increases in NaCl concentration in aqueous solution. DDI: doubly deionized water.

To evaluate accuracy, certified resistors (verified with a calibrated multimeter) were inserted at the R3 position. Voltage was sampled every second for 20 s, converted to resistance using the calibration equation, and compared to the true value. Percent recovery was computed as (measured resistance ÷ true resistance) × 100. Results from the three parallel sensors were averaged and are displayed in **Figure 2b**. At 22, 000 Ω, recovery ranged from 97.8% to 102.2%, yielding a relative standard deviation (RSD) of ±2.2%. Lower-value resistors showed even smaller error bars, indicating superior precision. Overall, these findings confirm high accuracy and reproducibility of the sensor.

The sensor's capacity to track rapid resistance changes in solution was then examined. As illustrated in **Figure 2c**, progressive addition of NaCl caused a steady decline in resistance, consistent with literature values for solution

impedance when adjusted for flow, electrode geometry, and surface area. The response was notably fast; for instance, raising NaCl from 0.01 M to 0.025 M required only ~5 s for stabilization. Across four replicates, the mean response time to concentration steps was 5.5 ± 1.29 s (mean ± standard deviation). These results highlight the sensor's suitability for high-temporal-resolution monitoring of dynamic TEER changes. At the conclusion of the test, electrodes were transferred directly to doubly deionized (DDI) water, producing the expected sharp resistance increase. Values in DDI water exceeded the upper limit and were flagged as overflow.

*Modular microfluidic platform for endothelium integration and TEER sensing*

The microfluidic device, fabricated by 3D printing, featured a cross-shaped internal channel **(Figure 3a)**. The central portion accommodated a rectangular cell-culture insert **(Figures 3b and 3c)** precoated with extracellular matrix to promote endothelial growth. Prior work from our group has shown that aligned microfibers better recapitulate native basement membrane topography and preserve physiological endothelial phenotype [30]. Accordingly, inserts were prepared with electrospun microfibers measuring 0.91 ± 0.16 μm in diameter (mean ± standard deviation, n = 15) and spaced 1.79 ± 0.44 μm apart (mean ± standard deviation, n = 15). The insert core was initially open (before fiber deposition) and remained permeable afterward to allow ion transport critical for reliable TEER readings [31-33].

An assembled system containing the cell-seeded insert and dual platinum electrodes is shown in **Figure 3d**. Endothelial cells formed confluent monolayers on the aligned fibers **(Figures 3e and 3f)**. To enable TEER measurement across the monolayer, the device incorporated two longitudinal ports that accepted the 3D-printed electrode holders, positioning platinum tips in contact with fluid on opposite sides of the insert. Epoxy tape could be applied around holders for added sealing if needed. The platform withstood continuous flow up to 4, 000 μL/min without leakage, spanning the full spectrum of physiologically relevant shear stresses and making it well-suited for endothelial mechanobiology studies [34, 35].

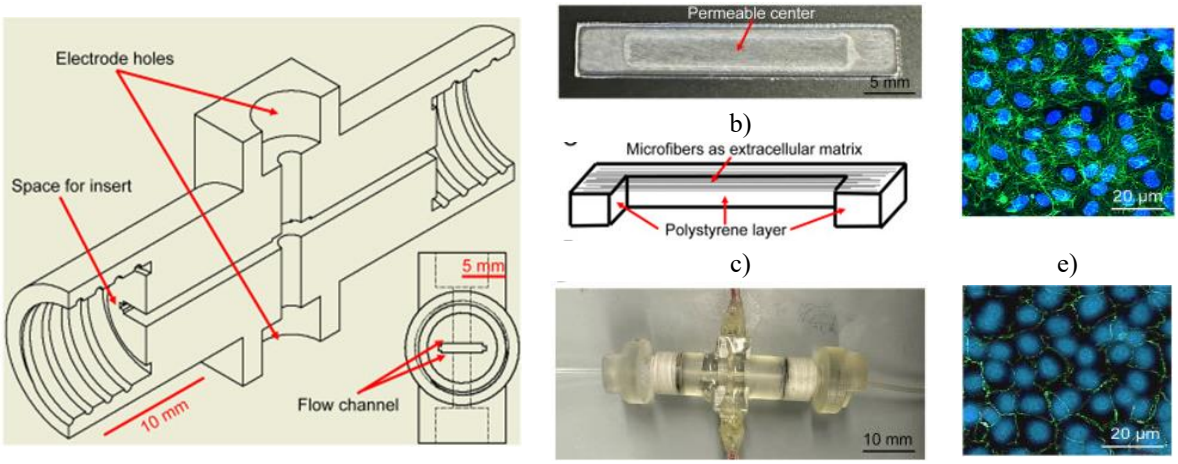


**Figure 3.** The 3D-printed modular microfluidic platform and associated cell-culture inserts. (a) Cross-sectional schematic showing electrode ports on opposite sides of the central channel for platinum electrode insertion. Threaded end ports accept fingertight tubing adapters. Inset: detailed view of the cross-shaped central channel housing the rectangular insert with aligned fibrous matrix supporting endothelial cells. Upper and lower arms allow media perfusion across both faces of the monolayer, with electrodes in contact. (b) Photograph of hollow inserts displaying the aligned microfiber layer (white) that mimics basement membrane architecture and supports endothelial phenotype maintenance. (c) Schematic cross-section of the insert illustrating fiber arrangement (not to scale) and top-side cell seeding. (d) Fully assembled device with cell insert, paired electrodes, and tubing adapters. (e) Confluent endothelial monolayer on microfibers within the integrated device (actin in green, DAPI nuclear stain in blue). (f) Confocal micrograph showing tight-junction protein occludin (green) and nuclei (blue) in the endothelial layer on the insert.

*Impact of doxorubicin on endothelial barrier function*

In recent years, endothelial toxicity from pharmaceutical agents has emerged as a critical area of study to better elucidate mechanisms of drug-induced cardiovascular damage [8, 36]. Monitoring the time-dependent alterations in endothelial permeability caused by therapeutic compounds provides essential insights for the safe clinical use

of doxorubicin—a potent anticancer agent widely recognized for its efficacy against tumors yet also implicated in direct endothelial cytotoxicity [37-39]. Although standard dosing guidelines for doxorubicin exist, its specific influence on endothelial barrier function—particularly under overdose conditions—remains poorly characterized, with few studies directly examining these effects [40, 41]. Consequently, doxorubicin was chosen as a model drug to probe potential disruptions to endothelial integrity.

Three identical platforms (each comprising a microfluidic device with embedded TEER sensor) were established inside a cell incubator, with DMEM medium perfused through each at 800 µL/min. Although the system supports flows up to 4, 000 µL/min, the selected rate produced a shear stress of 6.75 dyne/cm², mimicking conditions in large conduit arteries where endothelial impairment frequently contributes to cardiovascular pathology [42, 43]. The modular design of the microfluidic components, combined with the excellent reproducibility across TEER sensors, enabled simultaneous execution of three experimental conditions. This parallel approach improved throughput and data robustness, as endothelial cells across all devices originated from the same source vial and were seeded under identical conditions in a single Petri dish, isolating doxorubicin exposure as the sole variable.

As depicted in **Figure 4**, doxorubicin was added to the perfusion medium after 5 h of stable flow. Literature indicates that peak plasma concentrations during clinical doxorubicin administration typically fall between 0.5 and 1 µM [14, 36, 44]. Accordingly, 0.5 µM was employed as the therapeutic concentration, while 2.5 µM represented an overdose scenario. Upon introduction of the higher dose, endothelial TEER declined sharply, whereas the untreated control remained stable. After 24 h, monolayers exposed to 2.5 µM doxorubicin registered a TEER of 1, 728 ± 251 Ω·cm² (mean ± standard deviation), significantly lower than the 2, 875 ± 385 Ω·cm² observed in controls (mean ± standard deviation, n = 4; $P < 0.001$). This sustained reduction, initiating around 5 h post-exposure, showed no recovery, confirming marked increase in barrier permeability under excess drug levels. At the clinical dose of 0.5 µM, a modest TEER reduction to 2, 441 ± 449 Ω·cm² (mean ± standard deviation, n = 4) was noted after 24 h, yielding borderline significance versus control ($P = 0.0502$).

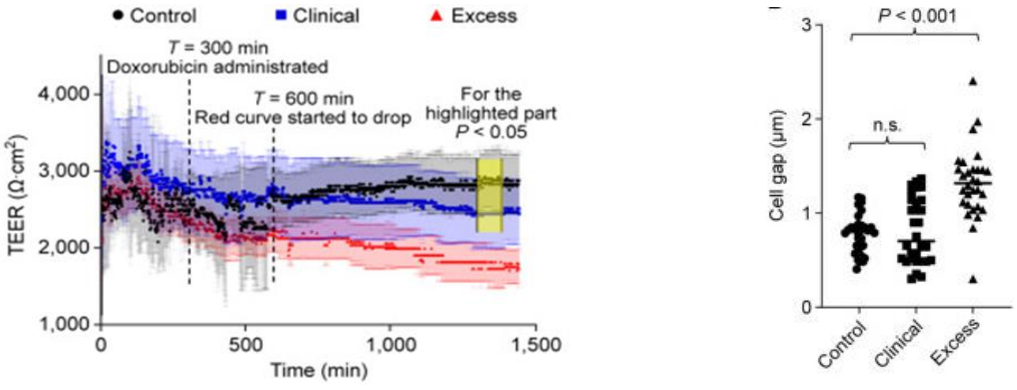


a) b)

**Figure 4.** Doxorubicin-induced changes in endothelial function detected by the platform. (a) Continuous 24-h TEER monitoring at 1-minute intervals. Control received no drug; doxorubicin was added after 300 min at 0.5 µM (clinical) or 2.5 µM (excess). Yellow shading marks periods of significant difference ($P < 0.05$) between control and clinical-dose curves. Excess-dose monolayers displayed pronounced TEER drop starting at T = 600 min, ending at 1, 728 ± 251 Ω·cm². Data represent n = 4 per condition; error bars = standard deviation. (b) Quantification of intercellular gaps post-TEER experiment across the three groups. n.s. denotes no significant difference.

Closer inspection of the 0.5 µM data revealed a statistically significant TEER decline ($P < 0.05$) beginning after 16 h and lasting ~90 min (highlighted region, **Figure 4a**). This perturbation proved transient, with subsequent recovery bringing p-values above 0.05 relative to controls.

To corroborate TEER findings, intercellular spacing was quantified after insert removal. Control monolayers exhibited the densest packing, with mean gaps of 0.78 ± 0.21 µm (mean ± standard deviation, n = 30). Clinical-dose samples showed comparable spacing of 0.81 ± 0.34 µm (mean ± standard deviation, n = 30), indicating preserved barrier function consistent with TEER results. In contrast, excess-dose treatment produced significantly wider gaps of 1.32 ± 0.37 µm (mean ± standard deviation, n = 30; $P < 0.001$ versus control), accompanied by

visible cellular damage. The divergent TEER trajectories between 0.5 μM and 2.5 μM highlight a clear concentration-dependent effect, evident in onset timing, magnitude of decline, and recovery behavior.
For the first time, we captured doxorubicin's influence on endothelial barrier properties at 1-minute resolution. Such kinetic detail would be unattainable without the present TEER system. Critically, experiments were conducted under physiologically relevant shear stress within a modular microfluidic environment featuring biomimetic extracellular matrix.

**Conclusion**

This work describes an enhanced design, fabrication, characterization, and biological application of an advanced TEER platform. Core advancements include an Arduino-driven customizable TEER sensor, a modular microfluidic system supporting endothelial culture on physiologically appropriate matrix, automated long-term recording with adjustable intervals, and capacity for parallel multi-condition experiments. Using this system, we elucidated doxorubicin's dynamic regulation of endothelial permeability at high temporal resolution, revealing previously undocumented near real-time behavior. The platform promises extensive further applications in drug-induced endothelial toxicity studies, offering substantial value to cardiovascular and pharmacological research fields.

**Acknowledgments:** None

**Conflict of Interest:** None

**Financial Support:** None

**Ethics Statement:** None

**References**

1. K.L. Audus, R.L. Bartel, I.J. Hidalgo, et al., The use of cultured epithelial and endothelial cells for drug transport and metabolism studies, Pharma Res. 7 (1990) 435e451.
2. L. Cacopardo, J. Costa, S. Giusti, et al., Real-time cellular impedance monitoring and imaging of biological barriers in a dual-flow membrane bioreactor, Bio-sens. Bioelectron. 140 (2019) 111340.
3. W.M. Pardridge, Drug and gene delivery to the brain: The vascular route, Neuron 36 (2002) 555e558.
4. L. Gonzalez-Mariscal, A. Betanzos, P. Nava, et al., Tight junction proteins, Prog. Biophys. Mol. Biol. 81 (2003) 1e44.
5. Y. Hashimoto, K. Tachibana, M. Kondoh, Tight junction modulators for drug delivery to the central nervous system, Drug Discov. Today 25 (2020) 1477e1486.
6. G. Nehra, B. Bauer, A.M.S. Hartz, Blood-brain barrier leakage in Alzheimer's disease: From discovery to clinical relevance, Pharmaco. Ther. 234 (2022), 108119.
7. S. Al-Bachari, J.H. Naish, G.J.M. Parker, et al., Bloodebrain barrier leakage is increased in Parkinson's disease, Front. Physiol. 11 (2020).
8. C.P. Profaci, R.N. Munji, R.S. Pulido, et al., The bloodebrain barrier in health and disease: Important unanswered questions, J. Exp. Med. 217 (2020).
9. A. Asif, S.H. Park, A. Manzoor Soomro, et al., Microphysiological system with continuous analysis of albumin for hepatotoxicity modeling and drug screening, J. Ind. Eng. Chem. 98 (2021) 318e326.
10. D.H. Elbrecht, C.J. Long, J.J. Hickman, Transepithelial/endothelial Electrical Resistance (TEER) theory and applications for microfluidic body-on-a-chip devices, J. Rare Dis. Res. Treat. 1 (2016).
11. B. Peyret, E. Crouzet, M. Mentek, et al., Integration of transepithelial electrical resistance (TEER) measurement in the corneal bioreactor, Acta Ophthalmol. 100 (2022).
12. B. Raut, L.-J. Chen, T. Hori, et al., An open-source add-on EVOM® device for real-time transepithelial/endothelial electrical resistance measurements in multiple transwell samples, Micromachines 12 (2021) 282.

13. C.G. Jones, T. Huang, J.H. Chung, et al., 3D-printed, modular, and parallelized microfluidic system with customizable scaffold integration to investigate the roles of basement membrane topography on endothelial cells, ACS Biomater. Sci. Eng. 7 (2021) 1600e1607.
14. B. Kalyanaraman, J. Joseph, S. Kalivendi, et al., Doxorubicin-induced apoptosis: Implications in cardiotoxicity, Mol. Cell. Biochem. 234 (2002) 119e124.
15. M. Theile, L. Wiora, D. Russ, et al., A simple approach to perform TEER measurements using a self-made volt-amperemeter with programmable output frequency, J. Vis. Exp. (2019) https://doi.org/10.3791/60087.
16. A. Moussawi, P. Ibrahim, B. Said, et al., Using Machine Learning to Enhance “Students' Assessment”, Dissertation, 2020.
17. B. Srinivasan, A.R. Kolli, M.B. Esch, et al., TEER measurement techniques for in vitro barrier model systems, J. Lab. Autom. 20 (2015) 107e126.
18. K. Benson, S. Cramer, H.-J. Galla, Impedance-based cell monitoring: Barrier properties and beyond, Fluids Barriers CNS 10 (2013), 5.
19. L.M. Griep, F. Wolbers, B. de Wagenaar, et al., BBB ON CHIP: Microfluidic platform to mechanically and biochemically modulate blood-brain barrier function, Biomed. Microdevices 15 (2013) 145e150.
20. T. Nitz, T. Eisenbl€atter, K. Psathaki, et al., Serum-derived factors weaken the barrier properties of cultured porcine brain capillary endothelial cells in vitro, Brain Res. 981 (2003) 30e40.
21. M.J. Cho, D.P. Thompson, C.T. Cramer, et al., The Madin Darby canine kidney (MDCK) epithelial cell monolayer as a model cellular transport barrier, Pharm. Res. 6 (1989) 71e77.
22. B. Zhang, J. Liang, C.L. Xu, et al., Electric double-layer capacitors using carbon nanotube electrodes and organic electrolyte, Mater. Lett. 51 (2001) 539e542.
23. I. Tanahashi, A. Yoshida, A. Nishino, Activated carbon fiber sheets as polarizable electrodes of electric double layer capacitors, Carbon 28 (1990) 477e482.
24. X. Yang, G. Zhang, Simulating the structure and effect of the electrical double layer at nanometre electrodes, Nanotechnology 18 (2007) 335201.
25. M.M. Saied, The analysis of bridge rectifier circuits using mathematica, Trends Electr. Eng. 10 (2020) 7e21.
26. S.G. Bratsch, Standard electrode potentials and temperature coefficients in water at 298.15 K, J. Phys. Chem. Ref. Data 18 (1989) 1e21.
27. A. Bard, Standard Potentials in Aqueous Solution, Routledge, 2017.
28. W. Ta, R. Hua, X. Li, et al., In vitro blood-brain barrier models from different species: An overview on permeability associated with drug delivery, J. Chin. Pharm. Sci. 32 (2023) 237e249.
29. J.P. Vigh, A. Kincses, B. Ozgür, et al., Transendothelial electrical resistance measurement across the bloodebrain barrier: A critical review of methods, Micromachines 12 (2021) 685.
30. S. Nagam Hanumantharao, N. Alinezhadbalalami, S. Kannan, et al., Electrospun acellular scaffolds for mimicking the natural anisotropy of the extracellular matrix, RSC Adv. 9 (2019) 40190e40195.
31. A. Abedi, M. Hasanzadeh, L. Tayebi, Conductive nanofibrous Chitosan/PEDOT: PSS tissue engineering scaffolds, Mater. Chem. Phys. 237 (2019) 121882.
32. T. Ahmad, J. Lee, Y.M. Shin, et al., Hybrid-spheroids incorporating ECM like engineered fragmented fibers potentiate stem cell function by improved cell/cell and cell/ECM interactions, Acta Biomater. 64 (2017) 161e175.
33. D.E.J. Anderson, M.T. Hinds, Extracellular matrix production and regulation in micropatterned endothelial cells, Biochem. Biophys. Res. Commun. 427 (2012) 159e164.
34. E. Roux, P. Bougaran, P. Dufourcq, et al., Fluid shear stress sensing by the endothelial layer, Front. Physiol. 11 (2020) 861.
35. C.M. Boulanger, N. Amabile, A.P. Guerin, et al., In vivo shear stress determines circulating levels of endothelial microparticles in end-stage renal disease, Hypertension 49 (2007) 902e908.
36. R.K. Hoffman, B.J. Kim, P.D. Shah, et al., Damage to cardiac vasculature may be associated with breast cancer treatment-induced cardiotoxicity, Cardio Oncol. Lond. Engl. 7 (2021) 15.
37. C. Carvalho, R.X. Santos, S. Cardoso, et al., Doxorubicin: The good, the bad and the ugly effect, Curr. Med. Chem. 16 (2009) 3267e3285.
38. C.F. Thorn, C. Oshiro, S. Marsh, et al., Doxorubicin pathways: Pharmacody-namics and adverse effects, Pharmacogenet. Genomics 21 (2011) 440.

39. S. Graziani, L. Scorrano, G. Pontarin, Transient exposure of endothelial cells to doxorubicin leads to long-lasting vascular endothelial growth factor receptor 2 downregulation, Cells 11 (2022) 210.
40. Y.I. Wang, H.E. Abaci, M.L. Shuler, Microfluidic bloodebrain barrier model provides in vivo-like barrier properties for drug permeability screening, Bio-technol. Bioeng. 114 (2017) 184e194.
41. E.L. Wilkinson, J.E. Sidaway, M.J. Cross, Cardiotoxic drugs Herceptin and doxorubicin inhibit cardiac microvascular endothelial cell barrier formation resulting in increased drug permeability, Biol. Open 5 (2016) 1362e1370.
42. J.D. Terwoord, A.M. Beyer, D.D. Gutterman, Endothelial dysfunction as a complication of anti-cancer therapy, Pharmacol. Ther. 237 (2022) 108116.
43. K.S. Cunningham, A.I. Gotlieb, The role of shear stress in the pathogenesis of atherosclerosis, Lab. Invest. 85 (2005) 9e23.
44. T. Wojcik, E. Buczek, K. Majzner, et al., Comparative endothelial profiling of doxorubicin and daunorubicin in cultured endothelial cells, Toxicol. Vitro 29 (2015) 512e521.